Available online at www.sciencedirect.com
SCIENCE DIRECT®
Journal of Sound and Vibration 281 (2005) 1077–1091
JOURNAL OF SOUND AND VIBRATION
www.elsevier.com/locate/jsvi

Vortex sound in the presence of a wedge with inhomogeneous surface flow impedance

S.K. Tang*, C.K. Lau

Department of Building Services Engineering, The Hong Kong Polytechnic University, Hung Hom, Kowloon, Hong Kong, P.R. China

Received 17 March 2003; received in revised form 1 December 2003; accepted 12 February 2004
Available online 29 September 2004

Abstract

The low Mach number vortex sound scattered by a sharp wedge formed by a rigid and an acoustically softer material is analyzed theoretically in the present investigation. A general expression for the time-varying far field potential due to the incompressible vortex motion around the edge of the wedge is derived to the leading order of magnitude. Results show that the introduction of a softer material increases the far field sound pulse magnitude. Also, it is found that the lower the impedance of the material, the louder the far field sound will be. In addition, it is shown that the effective fluid density inside the porous material is more important that the flow resistance in affecting the far field sound pulse magnitude when a weak vortex is concerned.

1. Introduction

The theory of Lighthill [1,2] shows explicitly the importance of turbulence as a source of low Mach number aerodynamic noise. Curle [3] extended this theory to include the effects of solid surfaces and showed that the noise radiated when a turbulent flow interacts with a solid surface is more important than that produced within the turbulent flow provided that the Mach number is low and the flow Reynolds number is high. The work of Ffowcs Williams and Hall [4] shows further the powerful radiation of sound by the scattering effect of a half-plane in the presence of a

*Corresponding author. Tel.: +852-2766-5847; fax: +852-2774-6146.
E-mail address: besktang@polyu.edu.hk (S.K. Tang).

0022-460X/$ - see front matter © 2004 Elsevier Ltd. All rights reserved.
doi:10.1016/j.jsv.2004.02.006

turbulent flow. Peake and Kerschen [5] investigated the sound generation by the interaction between a gust and a flat plate cascade. These theories are of great practical significance in engineering applications, especially when the noise control of ventilation systems is concerned.

Turbulence is hard to model so that many aerodynamic noise problems cannot be easily studied by using analytical methods. However, the situation becomes much simpler when the low Mach number turbulence is treated as discrete vortices because the dynamics of the latter can be obtained using the potential theory. The application of the vortex sound theory [6] or matched asymptotic expansion [7] then enables the estimation of the noise radiation. The use of vortices also facilitates the analysis of far field noise radiation due to flow singularity. Typical examples include the works of Crighton [7], Cannell and Ffowcs Williams [8], Howe [9] and Tang and Ko [10]. Though the vortices are drastic simplifications of a real turbulent flow, they can still provide useful insights to the topics, at least to the leading order of magnitude.

The flow inside a ventilation ductwork is in general turbulent and is of low Mach number. This turbulent flow, when it passes along the ductwork, will interact with the pipeline elements, such as splitters and dampers, to produce aerodynamic noise (for instance, see Nelson and Morfey [11]). Also, Ffowcs Williams [12] showed that noise can be generated by the turbulence over a sound absorbent lining, implying that the dissipative silencer used in building noise control is also a source of noise. Some flow junctions involve edges or are wedge-like and tend to scatter aerodynamic noise. However, a useful prediction model for these noises is, to the knowledge of the authors, not available in existing literature.

In the present study, the noise generated by a vortex filament moving in the vicinity of a sharp wedge having surfaces of different flow impedance is analyzed theoretically. Apart from generalizing the results of previous workers, it is hoped that the present results can provide a deeper insight into the aerodynamic noise generation inside air ductwork and useful information for the prediction of self-generated noise inside dissipative silencers [13].

2. Theoretical development

Fig. 1 shows the nomenclature used and the flow configuration for the present investigation. The wedge consists of two materials. One of the materials is assumed porous while the other is rigid for simplicity. The flow inside the porous material is governed by the effective density ρ_e and flow resistance R_f [14]. The former describes the inertial properties of the fluid in the pores of the material, and the latter the frictional retardation to flow through the pores. The flow equation within the porous material is, according to Morse and Ingard [14],

$$\rho_e \frac{\partial \mathbf{u}}{\partial t} + R_f \mathbf{u} + \nabla p = 0, \tag{1}$$

where $\mathbf{u}$ and p are the fluid velocity and fluid pressure inside the porous material. Here, we consider the noise radiated when a vortex filament with circulation Γ originally moving close to the rigid surface turns around the edge of the sharp wedge. The wedge angle α can vary between 0 and π. The strength of the vortex is assumed to be weak. All length scales in the present study are normalized by d_i, the initial perpendicular distance of the vortex from the rigid surface. The density of ambient fluid is denoted by ρ, such that the ratio ρ_e/ρ is always greater than unity.

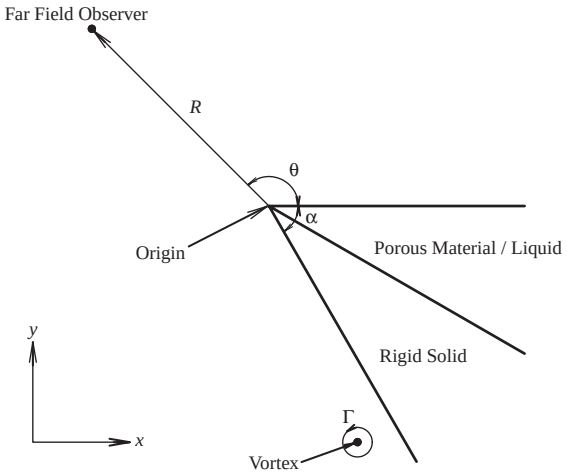

Fig. 1. Schematic diagram for the present vortex–wedge system (z-plane).

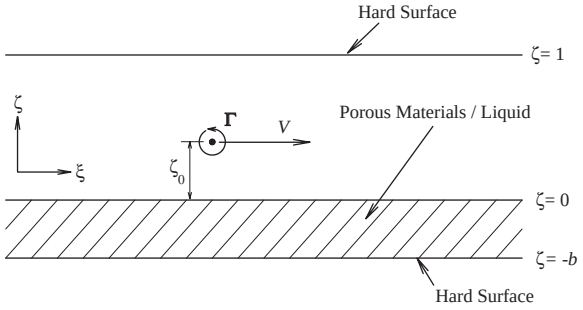

Fig. 2. Transformed complex w-plane.

According to the theories of Crighton [7] and Howe [9], the far field potential associated with the vortex motion can be estimated once the incompressible flow potential can be obtained. The analysis is started off by transforming the present vortex system (Fig. 1), which is hereafter referred to as the z-plane ($z = x + \mathrm{i}y$, $y \geqslant 0$), to a w-plane ($w = \xi + \mathrm{i}\zeta$), which is a parallel passage with $0 \leqslant \zeta \leqslant 1$ as shown in Fig. 2. The conformal mapping required is

$$z = \mathrm{e}^{(2\pi-\alpha)w}. \tag{2}$$

The branch cut in the z-plane is the positive x-axis. It has been shown by Tang [15] that the flow impedance is unaltered upon any conformal transformation. The streamfunction in the w-plane, ψ_w, can be obtained by the integration [15]:

$$\psi_w = \begin{cases} \frac{1}{4\pi}\int_{-\infty}^{\infty} \frac{\Gamma}{|k|}(\mathrm{e}^{-|k|\zeta} + g\mathrm{e}^{|k|\zeta})\frac{\mathrm{e}^{-|k|\zeta_0} - \mathrm{e}^{-2|k|}\mathrm{e}^{|k|\zeta_0}}{g+\mathrm{e}^{-2|k|}}\,\mathrm{e}^{\mathrm{i}k(\xi_0-\xi)}\,\mathrm{d}k, & \zeta < \zeta_0, \\ \frac{1}{4\pi}\int_{-\infty}^{\infty} \frac{\Gamma}{|k|}(\mathrm{e}^{-|k|\zeta_0} + g\mathrm{e}^{|k|\zeta_0})\frac{\mathrm{e}^{-|k|\zeta} - \mathrm{e}^{-2|k|}\mathrm{e}^{|k|\zeta}}{g+\mathrm{e}^{-2|k|}}\,\mathrm{e}^{\mathrm{i}k(\xi_0-\xi)}\,\mathrm{d}k, & \zeta \geqslant \zeta_0, \end{cases} \tag{3}$$

where $w_0 = \xi_0 + \mathrm{i}\zeta_0$ represents the position of the vortex in the w-plane and

$$g(k) = \frac{\mathrm{i}kV\rho + (\mathrm{i}kV\rho_e + R_f)\coth(|k|b)}{\mathrm{i}kV\rho - (\mathrm{i}kV\rho_e + R_f)\coth(|k|b)}, \tag{4}$$

where V is the velocity of the vortex in the w-plane, which is parallel to the ξ-axis and is a sole function of ζ_0. V can be calculated by differentiating Eq. (3) with respect to ζ. Details of the derivation of Eqs. (3) and (4) can be found in Tang [15] and are not repeated here. The flow potential in the w-plane, ϕ_w, is

$$\phi_w = \begin{cases} \frac{\mathrm{i}}{4\pi}\int_{-\infty}^{\infty} \frac{\Gamma}{k}(g\mathrm{e}^{|k|\zeta} - \mathrm{e}^{-|k|\zeta})\frac{\mathrm{e}^{-|k|\zeta_0} - \mathrm{e}^{-2|k|}\mathrm{e}^{|k|\zeta_0}}{g+\mathrm{e}^{-2|k|}}\,\mathrm{e}^{\mathrm{i}k(\xi_0-\xi)}\,\mathrm{d}k + C_l, & \zeta < \zeta_0, \\ \frac{-\mathrm{i}}{4\pi}\int_{-\infty}^{\infty} \frac{\Gamma}{k}(g\mathrm{e}^{|k|\zeta_0} + \mathrm{e}^{-|k|\zeta_0})\frac{\mathrm{e}^{-|k|\zeta} + \mathrm{e}^{-2|k|}\mathrm{e}^{|k|\zeta}}{g+\mathrm{e}^{-2|k|}}\,\mathrm{e}^{\mathrm{i}k(\xi_0-\xi)}\,\mathrm{d}k + C_u, & \zeta \geqslant \zeta_0, \end{cases} \tag{5}$$

where C_l and C_u are constants. It can be shown after some algebra that

$$\phi_w = \begin{cases} \frac{-\Gamma}{2\pi}\int_0^{\infty} \mathrm{Im}\left[\frac{1}{k}(g\mathrm{e}^{k\zeta} - \mathrm{e}^{-k\zeta})\frac{\mathrm{e}^{-k\zeta_0} - \mathrm{e}^{-2k}\mathrm{e}^{k\zeta_0}}{g+e^{-2k}}\,\mathrm{e}^{\mathrm{i}k(\xi_0-\xi)}\right]\mathrm{d}k + C_l, & \zeta < \zeta_0, \\ \frac{\Gamma}{2\pi}\int_0^{\infty} \mathrm{Im}\left[\frac{1}{k}(g\mathrm{e}^{k\zeta_0} + \mathrm{e}^{-k\zeta_0})\frac{\mathrm{e}^{-k\zeta} + \mathrm{e}^{-2k}\mathrm{e}^{k\zeta}}{g+\mathrm{e}^{-2k}}\,\mathrm{e}^{\mathrm{i}k(\xi_0-\xi)}\right]\mathrm{d}k + C_u, & \zeta \geqslant \zeta_0. \end{cases} \tag{6}$$

By observing that the flow potential vanishes as $\xi \to \pm\infty$, one finds for non-zero R_f that

$$C_l = \Gamma(\zeta_0 - 1)/2 \quad \text{and} \quad C_u = \Gamma\zeta_0/2. \tag{7}$$

Expressing z in polar form, $z = R\mathrm{e}^{\mathrm{i}\theta}$, where R is the distance of the vortex from the edge of the wedge (origin in the z-plane) and θ the angular position of the vortex in the z-plane, one obtains from Eq. (2) that

$$\xi = \frac{\ln R}{2\pi - \alpha}, \qquad \theta = (2\pi - \alpha)\zeta \quad \text{and} \quad b = \frac{\alpha/2}{2\pi - \alpha}. \tag{8}$$

Introducing the far field radius $r = MR$, where M is the Mach number of the flow, the far field potential due to the vortex motion can then be obtained by first substituting Eq. (8) and $R = r/M$ into Eq. (6), followed by taking $M \to 0$ as in Crighton [7].

3. Acoustically hard surfaces

The case for edges with acoustically hard surfaces has been investigated by several researchers, such as Crighton [7], Panaras [16] and Kambe [17]. However, the case for arbitrary wedge angle has not been explicitly presented. The condition of hard surfaces requires that $|-\mathrm{i}kV\rho_e + R_f| \gg |kV\rho|$ for all values of k, such that $g(k) = -1$ (Eq. (4)) and the final potential is independent of

b. The flow potential in the *w*-plane is, according to Eq. (6), given by

$$\phi_w = \begin{cases} \frac{\Gamma}{2\pi}\int_0^\infty \frac{1}{k}(e^{k\zeta}+e^{-k\zeta})\frac{e^{-k\zeta_0}-e^{-2k}e^{k\zeta_0}}{e^{-2k}-1}\sin(k(\xi_0-\xi))\,dk+\frac{\Gamma}{2}(\zeta_0-1), & \zeta<\zeta_0,\\ \frac{\Gamma}{2\pi}\int_0^\infty \frac{1}{k}(-e^{k\zeta_0}+e^{-k\zeta_0})\frac{e^{-k\zeta}+e^{-2k}e^{k\zeta}}{e^{-2k}-1}\sin(k(\xi_0-\xi))\,dk+\frac{\Gamma}{2}\zeta_0 & \zeta\geqslant\zeta_0,\end{cases}$$
$$= \begin{cases} \frac{\Gamma}{\pi}\int_0^\infty \cosh(k\zeta)\frac{\sinh(k(1-\zeta_0))}{k\sinh(k)}\sin(k(\xi-\xi_0))\,dk+\frac{\Gamma}{2}(\zeta_0-1), & \zeta<\zeta_0,\\ \frac{-\Gamma}{\pi}\int_0^\infty \sinh(k\zeta_0)\frac{\cosh(k(1-\zeta))}{k\sinh(k)}\sin(k(\xi-\xi_0))\,dk+\frac{\Gamma}{2}\zeta_0, & \zeta\geqslant\zeta_0.\end{cases} \tag{9}$$

Using the formula tabulated in Gradshteyn and Ryzhik [18], one obtains that for $\zeta_0>\zeta$,

$$\phi_w = \frac{\Gamma}{2\pi}\left\{\tan^{-1}\left[\tan\left(\frac{\pi}{2}(1-\zeta_0+\zeta)\right)\tanh\left(\frac{\pi}{2}(\xi-\xi_0)\right)\right] + \tan^{-1}\left[\tan\left(\frac{\pi}{2}(1-\zeta_0-\zeta)\right)\tanh\left(\frac{\pi}{2}(\xi-\xi_0)\right)\right]\right\}+\frac{\Gamma}{2}(\zeta_0-1) \tag{10a}$$

and for $\zeta_0\leqslant\zeta$,

$$\phi_w = \frac{-\Gamma}{2\pi}\left\{\tan^{-1}\left[\tan\left(\frac{\pi}{2}(1-\zeta+\zeta_0)\right)\tanh\left(\frac{\pi}{2}(\xi-\xi_0)\right)\right] - \tan^{-1}\left[\tan\left(\frac{\pi}{2}(1-\zeta_0-\zeta)\right)\tanh\left(\frac{\pi}{2}(\xi-\xi_0)\right)\right]\right\}+\frac{\Gamma}{2}\zeta_0. \tag{10b}$$

Substituting Eq. (8) into Eq. (10), the potential in the *z*-plane, ϕ, in polar form is for $\theta<\theta_0$,

$$\phi = \frac{\Gamma}{2\pi}\left\{\tan^{-1}\left[\cot\left(\frac{a(\theta_0-\theta)}{2}\right)\frac{R^a-R_0^a}{R^a+R_0^a}\right]+\tan^{-1}\left[\cot\left(\frac{a(\theta_0+\theta)}{2}\right)\frac{R^a-R_0^a}{R^a+R_0^a}\right]\right\}+\frac{a\Gamma\theta_0}{2\pi}-\frac{\Gamma}{2} \tag{11a}$$

where $a=\pi/(2\pi-\alpha)$. For $\theta\geqslant\theta_0$, one obtains

$$\phi = \frac{-\Gamma}{2\pi}\left\{\tan^{-1}\left[\cot\left(\frac{a(\theta-\theta_0)}{2}\right)\frac{R^a-R_0^a}{R^a+R_0^a}\right]-\tan^{-1}\left[\cot\left(\frac{a(\theta_0+\theta)}{2}\right)\frac{R^a-R_0^a}{R^a+R_0^a}\right]\right\}+\frac{a\Gamma\theta_0}{2\pi}. \tag{11b}$$

It can be shown that ϕ is continuous at $\theta=\theta_0$.

When $\alpha=\pi$, the wedge becomes an infinite flat surface and $a=1$. It can be shown exactly using sine rule that, for all θ,

$$\phi = \frac{\Gamma}{2\pi}\left[\tan^{-1}\left(\frac{R\sin\theta-R_0\sin\theta_0}{R\cos\theta-R_0\cos\theta_0}\right)-\tan^{-1}\left(\frac{R\sin\theta+R_0\sin\theta_0}{R\cos\theta-R_0\cos\theta_0}\right)\right]. \tag{12}$$

This is consistent with existing literature, for instance Lamb [19]. For large R, $\phi\to 0$.

For $0\leqslant\alpha<\pi$, $a<1$ and for $R\gg R_0$ and $\theta\geqslant\theta_0$, one can approximate Eq. (11b) as

$$\begin{aligned}\phi &\approx \frac{-\Gamma}{2\pi}\left\{\tan^{-1}\left[\cot\left(\frac{a(\theta-\theta_0)}{2}\right)\left(1-2\frac{R_0^a}{R^a}\right)\right]-\tan^{-1}\left[\cot\left(\frac{a(\theta_0+\theta)}{2}\right)\left(1-2\frac{R_0^a}{R^a}\right)\right]\right\}+\frac{a\Gamma\theta_0}{2\pi}\\ &= \frac{-\Gamma}{2\pi}\left\{\tan^{-1}\left[\cot\left(\frac{a(\theta-\theta_0)}{2}\right)\right]-\frac{R_0^a}{R^a}\sin(a(\theta-\theta_0))-\tan^{-1}\left[\cot\left(\frac{a(\theta+\theta_0)}{2}\right)\right]\right.\\ &\quad\left.+\frac{R_0^a}{R^a}\sin(a(\theta+\theta_0))\right\}+\frac{a\Gamma\theta_o}{2\pi}=-\frac{\Gamma}{\pi}\frac{R_0^a}{R^a}\cos(a\theta)\sin(a\theta_0).\end{aligned} \tag{13}$$

Exactly the same result can be obtained for $\theta<\theta_0$. This shows that there is a relatively strong radiation back to the downstream side where the wedge is located. For a rigid half plate occupying the region $x>0$, $y=0$ in the z-plane, $\alpha=0$ and $a=0.5$, and the far field potential becomes

$$\phi \approx -\frac{\Gamma}{\pi}\sqrt{\frac{R_0}{R}}\cos(\theta/2)\sin(\theta_0/2) = -\frac{\Gamma}{\pi}\sqrt{R_0}\,\sin(\theta_0/2)\sqrt{\frac{M}{r}}\cos(\theta/2). \tag{14}$$

For the case investigated by Crighton [7], the half-plane is located at $x<0$, $y=0$. The results of Crighton [7] can be obtained by rotating the present w-plane 180° in the anticlockwise direction. That is, by substituting θ and θ_0 in Eq. (14) by $\theta-\pi$ and $\theta_0-\pi$, respectively. The far field pressure can be estimated by differentiating ϕ in the far field with respect to the observer time t as in most references (for instance, Refs. [20,21]), where the unsteady Bernoulli equation with the constant density, ρ, are used. For $\alpha=\pi$, $a=1$ and such derivatives vanish as the vortex is moving parallel to the x-axis in the z-plane. Fig. 3 illustrates the far field pressure magnitude time variations at $R=100$ for different α while the directivity factor is ignored. The time t_a denotes the time at which the vortex passes across the axis of symmetry of the wedge. One can note that every far field pressure time variation contains a tail, which decays relatively slowly after the vortex passes over the edge of the wedge. This is typical for two-dimensional sound radiation due to the non-compactness of the source field so that sound generated from different parts of the source arrives at the far field at different instants. The rate of decay is slower at larger α. The larger the wedge angle α, the longer the sound radiation period. Also, both the tail and the far field pressure amplitude drop rapidly when α approaches 0. One should note that a increases with α so that the ratio $(R_0/R)^a$ actually decreases with increasing α for $R\gg R_0$. This implies that the sound generated with a rigid half-plane is more significant at large distance.

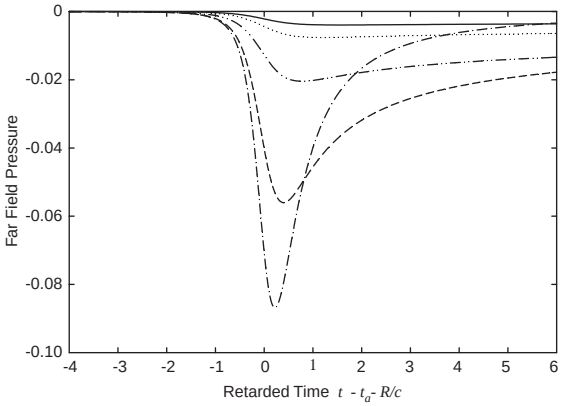

Fig. 3. Time variation of the sound pulse at $R=100$ for rigid wedge. —·—: $\alpha=0$; — —: $\alpha=\pi/3$; —··—: $\alpha=2\pi/3$; ····: $\alpha=5\pi/6$; ———: $\alpha=9\pi/10$.

4. Perfectly inviscid fluids

For a perfectly inviscid fluid, the flow resistance $R_f \equiv 0$. Eq. (4) then reduces to

$$g(k) = \frac{\rho + \rho_e \coth(|k|b)}{\rho - \rho_e \coth(|k|b)} = \frac{1 + m \coth(|k|b)}{1 - m \coth(|k|b)}, \tag{15}$$

where $m = \rho_e/\rho$. Since the equations for ϕ_w for $\zeta \geqslant \zeta_0$ and $\zeta < \zeta_0$ yield identical results, only the one for $\zeta \geqslant \zeta_0$ will be considered in the rest of the paper. The potential in the w-plane, according to Eq. (6), is

$$\phi_w = -\frac{\Gamma}{\pi} \int_0^\infty \frac{\cosh(k\zeta_0) + m \coth(kb) \sinh(k\zeta_0)}{\cosh(k) + m \coth(kb) \sinh(k)} \frac{\cosh(k(1-\zeta))}{k} \sin(k(\xi - \xi_0))\, \mathrm{d}k + C_u. \tag{16}$$

In this case, $C_u = \Gamma(m\zeta_0 + b)/2(m + b)$. We consider here the cases for $1 < m \leqslant 5$ when a porous material is concerned [14]. However, m can be large when the porous material is replaced by a heavier liquid ($\rho_e > \rho$).

In general, Eq. (16) is not easy to solve analytically. However, if $|\xi - \xi_0| \to \infty$, the solution can be approximated by considering the approximation for small k,

$$\cosh(k) \sinh(kb) + m \cosh(kb) \sinh(k) \approx m \sinh((m + b)k/m). \tag{17}$$

As an approximation, one can then write for finite b, $|\xi - \xi_0| \to \infty$ and $k' = k(\xi - \xi_0)$,

$$\begin{aligned} \phi_w &= -\frac{\Gamma}{\pi} \int_0^\infty \frac{\cosh(k\zeta_0) \sinh(kb) + m \cosh(kb) \sinh(k\zeta_0)}{\cosh(k) \sinh(kb) + m \cosh(kb) \sinh(k)} \frac{\cosh(k(1-\zeta))}{k} \sin(k(\xi - \xi_0))\, \mathrm{d}k + C_u, \\ &\approx -\frac{\Gamma}{m\pi} \int_0^\infty \frac{(m+1)\sinh(k(\zeta_0 + b)) + (m-1)\sinh(k(\zeta_0 - b))}{\sinh\big((m+b)k/m\big)} \frac{\cosh(k(1-\zeta))'}{k} \sin(k')\, \mathrm{d}k' + C_u. \end{aligned} \tag{18}$$

Eq. (18) can be solved analytically, even when $m \to 0$, using the formula shown in Gradshteyn and Ryzhik [18], and for $|\xi - \xi_0| \to \infty$ one obtains

$$\phi_w = \frac{\Gamma}{\pi} \sin\left(\frac{m\pi\zeta_0}{m+b}\right) \cos\left(\frac{m\pi}{m+b}(1-\zeta)\right) \exp\left(-\frac{m\pi(\xi - \xi_0)}{m+b}\right). \tag{19}$$

Fig. 4 shows that Eq. (19) agrees well with the results obtained from direct numerical integration of Eq. (16). The comparison is not extended to the range $\xi - \xi_0 > 4$ as ϕ_w will be too small to be handled accurately in the numerical integration. However, one can note from the conformal mapping adopted that the ratio R/R_0 is already very large when $\xi - \xi_0 = 4$. After applying the conformal mapping (Eq. (7)), one obtains

$$\begin{aligned} \phi_w &= \frac{\Gamma}{\pi} \sin\left(\frac{m\pi\theta_0}{m(2\pi - \alpha) + \alpha/2}\right) \cos\left(\frac{m\pi}{m(2\pi - \alpha) + \alpha/2}(2\pi - \alpha - \theta)\right) \left(\frac{R_0}{R}\right)^{m\pi/(m(2\pi-\alpha)+\alpha/2)} \\ &= -\frac{\Gamma}{\pi} \sin\left(\frac{m\pi\theta_0}{m(2\pi - \alpha) + \alpha/2}\right) \cos\left(\frac{m\pi(\theta + \alpha/2m)}{m(2\pi - \alpha) + \alpha/2}\right) \left(\frac{R_0}{R}\right)^{m\pi/(m(2\pi-\alpha)+\alpha/2)}. \end{aligned} \tag{20}$$

Eq. (20) reduces to Eq. (13) for large m. For $m = 1$, there is no porous surface. The situation then reduces to that of a wedge with wedge angle $\alpha/2$ and rigid surfaces. Eqs. (16) and (20) give

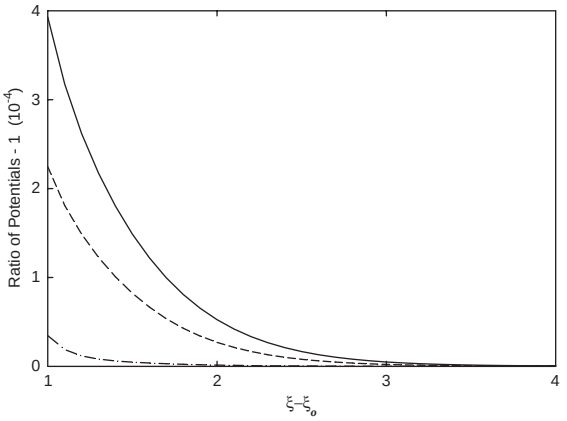

Fig. 4. Accuracy of the approximation of Eq. (19). ———: $m = 2$; — —: $m = 5$; — · —: $m = 100$.

the same result as that obtained from Eq. (13), by taking the wedge angle to be $\alpha/2$ instead of α and rotating the far field anticlockwise by $\alpha/2$. Though m is not likely to be less than unity, Eq. (20) tends to suggest that the magnitude of the far field pressure decreases should such a pressure-releasing surface exist. For $m = 0$, there will be no sound radiation. Fig. 5 summarizes the effect of m on the far field radiation directivity. It is expected that the introduction of a pressure-releasing surface allows more sound radiation in a direction closer to this surface. The larger the wedge angle or the smaller the value of m, the greater this shift will be.

The far field pressure magnitudes for some values of m at $\alpha = \pi$ are shown in Fig. 6. This case has been investigated by Tang and Li [22] on the assumption that the frequency of the radiated sound is so low that the impedance surface has no effect on the sound radiation. Thus, only the dipole radiation was considered in Tang and Li [22]. As expected, the scattered sound field becomes weaker as m increases from unity and the rate of such weakening decreases considerably quickly for some m. The magnitudes of the sound fields are higher than those shown in Tang and Li [22]. Together with the fact that the present scattered field magnitude varies with M^a where a is less than unity, the scattered field is much stronger than the dipole radiation in Tang and Li [22].

For α less than π, the vortex moves towards the pressure-releasing surface after it passes over the edge of the wedge. Fig. 7 shows the vortex paths at $m = 2$, 4 and ∞ for $\alpha = \pi/3$. The initial vortex position is at one unit length perpendicular to the hard surface at $R_0 \approx 100$. It can be noted that the smaller the value of m, the closer the vortex will be to the pressure-releasing surface eventually. Fig. 8 shows the sound pressure time fluctuations for finite m at $R = 100$. These patterns are basically similar to those for rigid surfaces (Fig. 3). However, one can note that the peak pressure is higher for smaller m. The tail of the sound pressure fluctuation pattern becomes shorter as m decreases, implying shorter period for active and significant sound production at smaller m. The power associated with the radial radiation term $1/R$ is $m\pi/(m(2\pi - \alpha) + \alpha/2)$, which increases with m. The far field sound, therefore, decays more rapidly at increasing m.

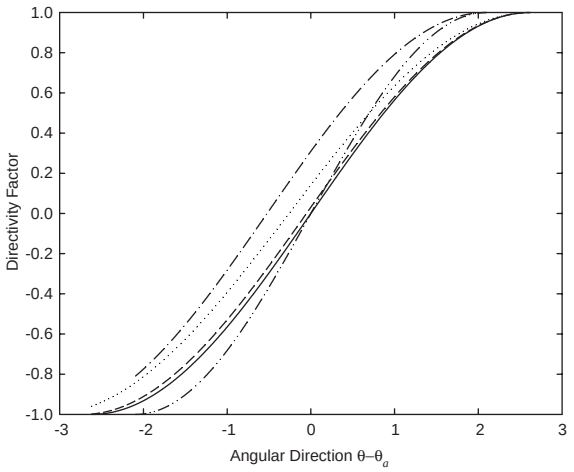

Fig. 5. Effect of effective fluid density on the radiation directivity for a perfectly inviscid medium. · · · ·: $m = 1$, $\alpha = \pi/3$; — —: $m = 5$, $\alpha = \pi/3$; ———: rigid wedge, $\alpha = \pi/3$; — · —: $m = 1$, $\alpha = 2\pi/3$; — · · —: rigid wedge, $\alpha = 2\pi/3$.

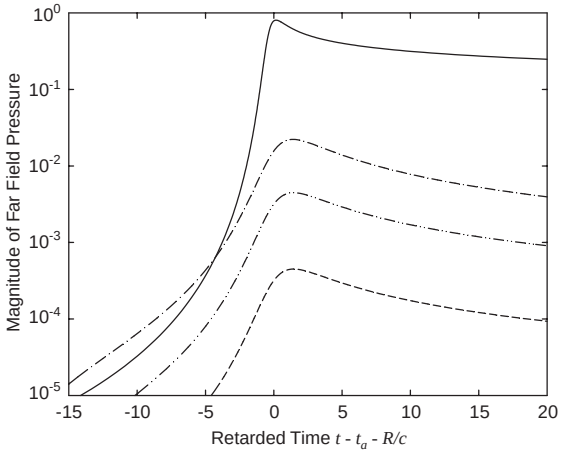

Fig. 6. Effect of effective fluid density on sound pressure fluctuations for perfectly inviscid medium. ———: $m = 1$; — · —: $m = 20$; — · · · —: $m = 100$; — —: $m = 1000$. $\alpha = \pi/3$.

Similar results are obtained at different α ($<\pi$). The effect of wedge angle on the sound radiation is summarized in Fig. 9. Again, the magnitude of the sound pulse increases with decreasing α.

5. Combined effects of m and R_f

For a real porous material, R_f is finite and m varies from 1 to about 3 [14]. The far field potential ϕ_w can be obtained from Eqs. (5) and (6). Again, we consider the case for $\zeta \geqslant \zeta_0$ and let

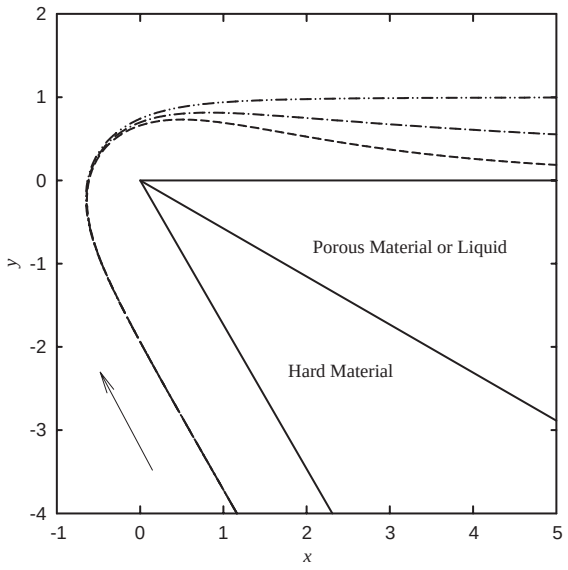

Fig. 7. Vortex flight path in a perfectly inviscid medium. — —: $m = 2$; —·—: $m = 4$; —· ·—: rigid wedge. $\alpha = \pi/3$.

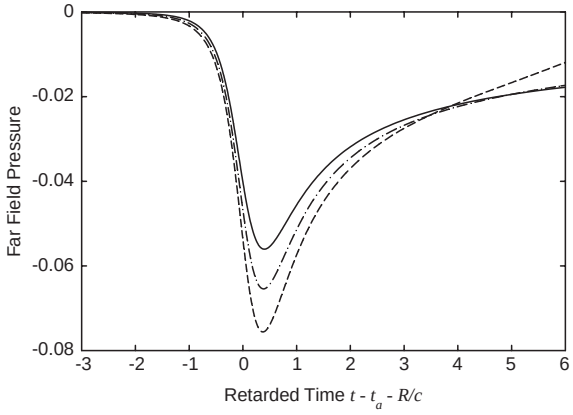

Fig. 8. Sound pressure time variation for finite m at $R = 100$, $\alpha = \pi/3$. — —: $m = 2$; —·—: $m = 4$; ———: rigid wedge.

$k' = k(\xi - \xi_0)$, one obtains

$$\phi_w = \frac{\Gamma}{\pi}\left(\int_0^\infty \mathrm{Im}(G(k))\cos(k')/k'\,\mathrm{d}k' - \int_0^\infty \mathrm{Re}(G(k))\sin(k')/k'\,\mathrm{d}k'\right) + \frac{\Gamma\zeta_0}{2}, \tag{21}$$

where

$$G = \frac{\mathrm{i}kV\rho\,\cosh(k\zeta_0)\sinh(kb) + (\mathrm{i}kVm\rho + R_f)\cosh(kb)\sinh(k\zeta_0)}{\mathrm{i}kV\rho\,\cosh(k)\sinh(kb) + (\mathrm{i}kVm\rho + R_f)\cosh(kb)\sinh(k)}\cosh(k(1-\zeta)). \tag{22}$$

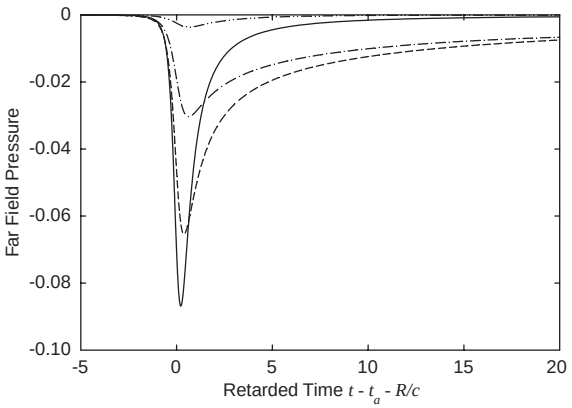

Fig. 9. Effect of wedge angle on the sound pulse magnitude. ———: $\alpha = 0$; — —: $\alpha = \pi/3$; —·—: $\alpha = 2\pi/3$; —· ·—: $\alpha = \pi$. $m = 4$.

It can be shown that

$$G = \left(\frac{\mathrm{i}kV\rho(\coth(k\zeta_0) - \coth(k))}{\mathrm{i}kV\rho(\coth(k) + m\coth(kb)) + R_f \coth(kb)} + 1 \right) \frac{\sinh(k\zeta_0)\cosh(k(1-\zeta))}{\sinh(k)}. \tag{23}$$

Again, the analytical solution for Eq. (21) is hard to find without assumption. As we are interested in the far field where $|\xi - \xi_0| \to \infty$, ϕ_w then depends on the value of G as $k \to 0$, which is unity. One can thus conclude to the leading order of magnitude that

$$\phi_w \approx -\frac{\Gamma}{\pi} \int_0^\infty \mathrm{Re}(G(k)) \sin(k')/k' \, \mathrm{d}k' + \frac{\Gamma\zeta_0}{2} \Rightarrow \phi = -\frac{\Gamma}{\pi} \frac{R_0^a}{R^a} \cos(a\theta) \sin(a\theta_0). \tag{24}$$

The directivity of sound radiation for non-vanishing R_f is the same as that with hard surfaces or at large m.

Fig. 10 illustrates the combined effects of m and R_f on the vortex path. In general, the vortex propagates towards the porous surface soon after it passes over the edge of the wedge. It is observed that the larger the value of m or R_f, the less serious the bending of the vortex path will be. The increase in the flow resistance R_f makes the porous surface less pressure-releasing and produces the same effect as increasing m. In Fig. 11 the far field sound pressure fluctuations at $R = 100$ for $\alpha = \pi/3$ and $m = 2$ are shown. The increase in R_f reduces the magnitude of the pulse. The less severe vortex path bending towards the porous surface at larger R_f and m results in smaller vortex acceleration and thus weaker sound radiation. It is found that the magnitude of the sound pulse increases as m decreases when R_f is fixed (not shown here). However, the variation becomes insignificant for $4\pi d_i^2 R_f/\rho\Gamma \geqslant 100$. The increase in the wedge angle α again reduces the magnitude of the sound pulse, but the far field sound fluctuation patterns are very similar to those shown in Fig. 9 and thus are not presented.

Fig. 12 summarizes the combined effects of α, m and R_f on this pulse magnitude. These magnitudes are normalized by those with hard surfaces so that the effect of R can be ignored.

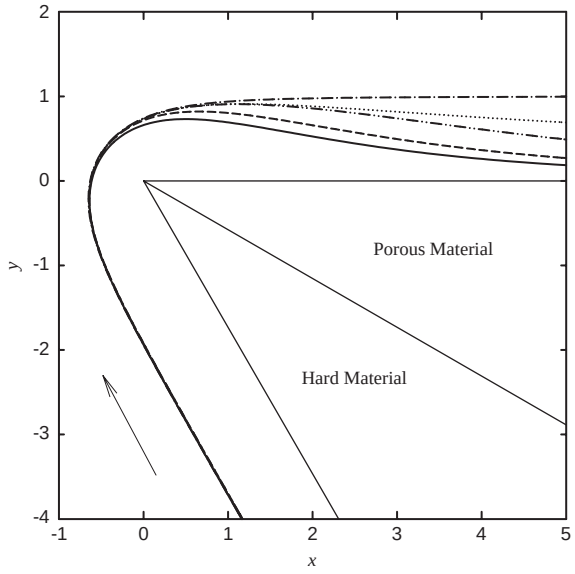

Fig. 10. Combined effects of effective fluid density and flow resistance on the vortex path. ———: $m = 2$, $4\pi d_i^2 R_f/\rho\Gamma = 0$; — —: $m = 2$, $4\pi d_i^2 R_f/\rho\Gamma = 10$; —· ·—: $m = 2$, $4\pi d_i^2 R_f/\rho\Gamma = 100$; · · · · · · : $m = 4$, $4\pi d_i^2 R_f/\rho\Gamma = 100$; —·—: rigid wedge. $\alpha = \pi/3$.

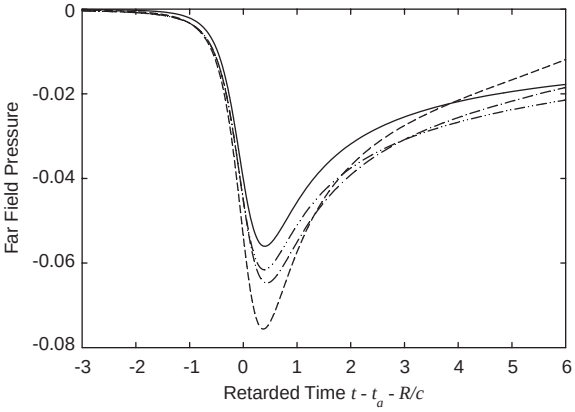

Fig. 11. Effect of flow resistance on the far field sound radiation. — —: $4\pi d_i^2 R_f/\rho\Gamma = 0$; —·—: $4\pi d_i^2 R_f/\rho\Gamma = 10$; —· ·—: $4\pi d_i^2 R_f/\rho\Gamma = 100$; ———: rigid wedge. $m = 2$, $\alpha = \pi/3$.

Again, one can observe that louder sound radiation resulted from the introduction of a porous material. This is the result of the increase of porous material thickness with wedge angle so that the pressure-supporting interface between the porous and the rigid materials becomes less influential.

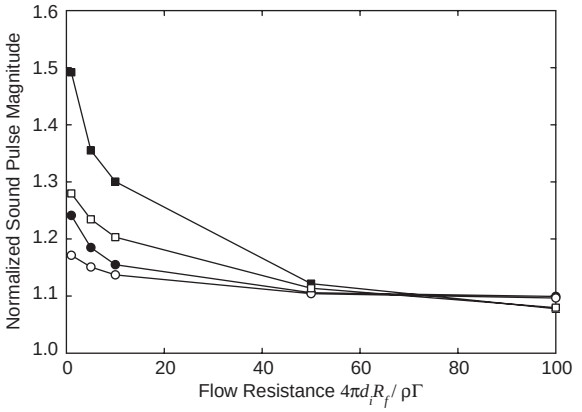

Fig. 12. Combined effects of effective fluid density, flow resistance and wedge angle on sound radiation. ●: $m = 2$, $\alpha = \pi/3$; ○: $m = 2$, $\alpha = 2\pi/3$; ■: $m = 4$, $\alpha = \pi/3$; □: $m = 4$, $\alpha = 2\pi/3$.

6. Conclusions

The sound field produced by a vortex engaging the edge of a wedge with inhomogeneous surface impedance is investigated theoretically in the present study. The wedge is made up symmetrically of a rigid material and an acoustically softer material, which can be a porous material or a heavy liquid. The initial location of the vortex is on the rigid material side far away from the edge of the wedge. The effects of the wedge angle, the effective fluid density and flow resistance of the softer material on the directivity and magnitude of the far field sound are discussed. A general expression for the leading order approximation of the sound field is derived.

In all cases studied, the far field sound is a pulse whose magnitude decreases with increasing wedge angle. The time variation of each pulse contains a tail which is typical for two-dimensional sound radiation. The rate of decay of the pulse increases as the wedge angle increases. When the wedge edge is fixed, the magnitude of the far field pulse decreases as the solid surface becomes more acoustically hard. The vortex path bends towards the impedance surface after it passes over the edge of the wedge when the surface impedance is reduced, resulting in high vortex acceleration and thus stronger sound radiation. The final velocity of the vortex is higher than that in the hard surface case.

In a perfectly inviscid fluid medium, the far field sound is only affected by the effective fluid density and the wedge angle. It is found that a finite effective fluid density deflects the directivity towards the softer surface. The extent of such deflection increases with increasing effective fluid density. However, the rate of decay of the sound pulse with distance from the edge is lower if the effective fluid density is reduced. The introduction of a porous surface in a perfectly inviscid fluid results in louder and more distant noise radiation.

When the fluid possesses non-vanishing viscosity, the flow resistance inside the lattice of the porous material becomes significant. The higher the flow resistance, the higher the ability of the porous surface to support pressure, resulting in weaker sound pulse in the far field. However,

unlike the effect of the effective fluid density, the directivity and the rate of decay of the sound radiation in the leading order of magnitude are the same as those with hard surfaces, regardless of the magnitude of the flow resistance.

Acknowledgements

The financial support from the Research Grants Council, The Hong Kong Special Administration Region Government, China (Project PolyU5030/00E) is gratefully acknowledged. The authors would also like to thank Dr N Peake of the Department of Applied Mathematics and Theoretical Physics, the University of Cambridge for his constant interest in the topic.

References

[1] M.J. Lighthill, On sound generated aerodynamically. I. General theory, *Proceedings of the Royal Society of London, Series A* 211 (1952) 564–587.
[2] M.J. Lighthill, On sound generated aerodynamically. II. Turbulence as a source of sound, *Proceedings of the Royal Society of London, Series A* 222 (1954) 1–32.
[3] N. Curle, The influence of solid boundaries upon aerodynamic sound, *Proceedings of the Royal Society of London, Series A* 231 (1955) 505–514.
[4] J.E. Ffowcs Williams, L.H. Hall, Aerodynamic sound generation by turbulent flow in the vicinity of a scattering half-plane, *Journal of Fluid Mechanics* 40 (1970) 657–670.
[5] N. Peake, E.J. Kerschen, Influence of mean loading on noise generated by the interaction of gusts with a flat-plate cascade: upstream radiation, *Journal of Fluid Mechanics* 347 (1997) 315–346.
[6] A. Powell, Vortex sound theory, *Journal of Acoustical Society of America* 36 (1964) 177–195.
[7] D.G. Crighton, Radiation from vortex filament motion near a half-plane, *Journal of Fluid Mechanics* 51 (1972) 357–362.
[8] P. Cannell, J.E. Ffowcs Williams, Radiation from line vortex filaments exhausting from a two-dimensional semi-infinite duct, *Journal of Fluid Mechanics* 58 (1973) 65–80.
[9] M.S. Howe, Contributions to the theory of aerodynamic sound, with application to excess jet noise and the theory of the flute, *Journal of Fluid Mechanics* 71 (1975) 625–673.
[10] S.K. Tang, N.W.M. Ko, Basic sound generation mechanisms in inviscid vortex interactions at low Mach number, *Journal of Sound and Vibration* 262 (2003) 87–115.
[11] P.A. Nelson, C.L. Morfey, Aerodynamic sound production in low speed flow ducts, *Journal of Sound and Vibration* 79 (1981) 263–289.
[12] J.E. Ffowcs Williams, The acoustics of turbulence near sound-absorbent liners, *Journal of Fluid Mechanics* 51 (1972) 737–749.
[13] L.L. Beranek, *Noise and Vibration Control Engineering, Principles and Applications*, Wiley, New York, 1992.
[14] P.M. Morse, *U.K. Ingard, Theoretical Acoustics*, McGraw-Hill, New York, 1968.
[15] S.K. Tang, Effects of porous boundaries on the dynamics of an inviscid vortex filament, *Quarterly Journal of Mechanics and Applied Mathematics* 54 (2001) 65–84.
[16] A.G. Panaras, Pressure pulses generated by the interaction of a discrete vortex with an edge, *Journal of Fluid Mechanics* 154 (1985) 445–461.
[17] T. Kambe, Acoustic emissions by vortex motions, *Journal of Fluid Mechanics* 173 (1986) 643–666.
[18] I.S. Gradshteyn, I.M. Ryzhik, *Table of Integrals, Series, and Products*, Academic Press, London, 1980.
[19] H. Lamb, *Hydrodynamics*, Cambridge University Press, Cambridge, 1993.

[20] D.G. Crighton, A.P. Dowling, J.E. Ffowcs Williams, M. Heckl, F.G. Leppington, *Modern Methods in Analytical Acoustics*, Springer, London, 1992.
[21] F. Obermeier, On a new representation of aeroacoustic source distribution II. Two-dimensional model flows, *Acustica* 42 (1979) 62–71.
[22] S.K. Tang, K.M. Li, Vortex sound generation due to a flow impedance discontinuity on a flat surface, *Journal of the Acoustical Society of America* 109 (2001) 1334–1341.